Results in Engineering 16 (2022) 100687

Contents lists available at ScienceDirect

Results in Engineering

journal homepage: www.sciencedirect.com/journal/results-in-engineering

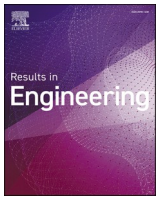

Modeling and scaling up of the Cr(VI) adsorption process by using mexicalcite natural mineral in a packed bed column

Julian Cruz-Olivares [a,b,*], César Pérez-Alonso [a], Gonzalo Martínez-Barrera [c], Gabriela Roa-Morales [d], Gustavo López-Téllez [d], Eduardo Martín del Campo-López [a]

[a] Facultad de Química, Universidad Autónoma del Estado de México, Paseo Colón Esq, Paseo Tollocan S/N, 50120, Toluca, Estado de México, Mexico
[b] MCCM Ciencia e Innovación Tecnológica S.A, de C.V. Av. Benito Juárez Sur 1002, Col. Universidad, C.P. 50130, Toluca, Estado de México, Mexico
[c] Laboratorio de Investigación y Desarrollo de Materiales Avanzados (LIDMA), Facultad de Química, Universidad Autónoma del Estado de México, Km.12 de la carretera Toluca-Atlacomulco, San Cayetano, 50200, Mexico
[d] Centro Conjunto de Investigación en Química Sustentable UAEM-UNAM, (CCIQS), Carretera Toluca-Atlacomulco Km 14.5, Unidad El Rosedal, Toluca, Estado de México, CP, 50200, Mexico

ARTICLE INFO

Keywords:
Cr (VI) removal
Packed bed column
BDST model
Scaling adsorption process

ABSTRACT

The natural mineral known as Mexicalcite is native to the southern region of Mexico, and due to its abundance and accessibility characteristics, as well as its insolubility in water, it is recommended as an adsorbent material. For such reasons, in this work Mexicalcite was used as adsorbent material to remove Cr(VI) in a packed bed column. The effects of the parameters: bed column height (Z), flow rate (Q), and the initial chromium concentration (C_0), on the adsorption capacity (q) and removal percentage (%R) were evaluated. The results show minimal changes in adsorption capacity, specifically a 4% difference; with a mean value of 4.98 mg/g. However, maximum removal percentage was obtained for a high height in the bed column, where there is more contact time. However, low removal percentages were obtained for high flow rate, where the contact time is considerably less. The maximum removal was 94.09%, which was obtained with the highest packed bed height ($Z = 6$ cm), initial concentration ($C_0 = 25$ mg/L), and lowest flow rate ($Q = 2$ mL/min). The process was modeled using the Thomas, Adams-Bohart and Yoon-Nelson models. With the BDST model, it was possible to scale up the adsorption process and double the original column dimensions. In addition, the column dimensions were obtained theoretically, to operate continuously for 120 h. Finally, the chromium concentration at the outlet was 0.1 mg/L, using a value of 2 for the bed height/column diameter ratio (Z/d).

1. Introduction

In Mexico, water contamination with chromium ions is produced by the metal coating and leather tanning industries, which do not have regulated treatments for contaminated water, in violation of governmental environmental regulations. Therefore, there are serious health risks for employees and people living in the vicinity of the industries. In addition, prolonged contact with Cr(VI) ions can cause damage to the respiratory tract, eyes and skin or, in severe cases, mutagenic, genotoxic and reproductive effects; it is even possible to develop cancer of the brain, lungs, stomach, liver or kidneys [1–4].

There are several technologies to remove chromium from wastewater, such as chemical precipitation and coagulation, ion exchange, extraction, membrane ultrafiltration, electrochemical methods, photochemical oxidation processes, biological treatments and adsorption [5,6]. Either because of their high operating or investment cost, their inefficiency or their high environmental impact, most of them are not widely used. Adsorption, and in particular bioadsorption, is by far the most widely used technology, mainly because it is considered an easy, efficient and environmentally friendly method, and because low-cost adsorbent materials are used; usually from agricultural waste [7,8]. Most of these bioadsorbents have a high adsorption capacity and a high removal rate [9,10]. The highest values have been reported in batch type processes. For example, for Cr(VI) removal, walnut shell and almond shell showed adsorption capacities higher than 24 mg/g [11]. From the comparative tables reported by several authors, mango leaves,

* Corresponding author. Facultad de Química, Universidad Autónoma del Estado de México, Paseo Colón esq, Paseo Tollocan S/N, 50120, Toluca, Estado de México, Mexico.
E-mail address: jcruzo@uaemex.mx (J. Cruz-Olivares).

https://doi.org/10.1016/j.rineng.2022.100687
Received 25 July 2022; Received in revised form 23 September 2022; Accepted 4 October 2022
Available online 7 October 2022

eucalyptus bark and macadamia nut shell stand out, which showed adsorption capacities of 35.7, 45.0 and 45.23, respectively [11,12]. As a disadvantage, it can be mentioned that bioadsorbents, when put in contact with water, tend to agglomerate, causing large pressure drops and clogging in packed columns, since they are basically composed of cellulose, hemicellulose and lignin.

On the other hand, there are inorganic adsorbents, such as polymeric membranes, calcite-type minerals, clays, silicoaluminates and natural or synthetic zeolites. In general, these adsorbent materials can be as efficient, in terms of adsorption capacity and percentage removal, as bioadsorbents, especially when their structure is physically or chemically modified [13,14]. For example, for Cr(VI) adsorption, a clinoptilolite modified with octadecylammonium has shown an adsorption capacity of 54 mg/g [13], for magnetic calcite an adsorption capacity of 24.2 mg/g has been reported [15], these values are substantially higher than those shown by the same unmodified adsorbents.

Natural inorganic adsorbents, such as Mexicalcite, are abundant and inexpensive and have the advantage of being insoluble in water, having a low swelling index and good mechanical strength properties. In addition, they do not require sophisticated treatments before being used as adsorbents. Therefore, these materials are preferred as adsorbents in continuous packed column processes.

The materials used as adsorbents require previous treatments to improve their functionality. In the case of bioadsorbents, these treatments consist first in the removal of soluble organic matter, for which aqueous solutions of sodium hydroxide, sulfuric acid, nitric acid or hydrochloric acid are used, then they are washed with water and finally subjected to the drying and sieving process [16,17]. In the case of inorganic adsorbents, the previous treatment is simpler, only requiring washing with hot water, drying and sieving. However, in both cases, structural modifications can be performed by physical processes [18] or chemical reactions [19] to improve the selectivity and adsorption capacity.

The mechanism of the adsorption process can be explained by analyzing the physicochemical properties of the adsorbent before and after adsorption. By Fourier transform infrared spectroscopy (FTIR) the chemical composition is determined by identifying the functional group of the molecule responsible for adsorption, with scanning electron microscopy (SEM) it is possible to determine the morphology and by energy dispersive spectroscopy (EDS) the elemental analysis of the adsorbent is known [20].

Adsorption technologies used for the removal of chromium ions have proven effective at laboratory scale, but not on a large scale such as those involving industrial processes. For this reason, modeling and scale-up studies are performed on continuous rather than batch processes; moreover, industrial wastewater is used instead of synthetic water.

There are many options for modeling the column adsorption process when laboratory-scale data are collected, and breakthrough curves are available. The most commonly used models for analyzing column behavior in terms of adsorbent-adsorbate system interaction are Thomas model, Bed Depth Service Time model, Adams-Bohart model, dose-response model, among others. These models are used because they adequately describe the dynamics of the column adsorption process, since they assume that there is axial dispersion, external mass transfer, intraparticle diffusion and that the isotherms describing the phenomenon are nonlinear [20]. The considerations for the use of these models in column adsorption processes have been described in previous works [18,21], and their equations are shown below.

I) Thomas model

$$Ln\left(\frac{C_0}{C_t}-1\right)=\frac{K_{Th}q_0w}{Q}-K_{Th}C_0t \tag{1}$$

where C_0 and C_t are the chromium concentrations (mg/L), measures at the inlet and outlet of the column, K_{Th} is the Thomas constant (mL/mg·min), q_0 is the adsorption capacity (mg/g), w is the mass of adsorbent (g), Q is the volumetric flow (mL/min) and t is time (min).

II) Adams – Bohart model

$$Ln\left(\frac{C_t}{C_0}\right)=K_{AB}C_0t-K_{AB}N_0\left(\frac{Z}{v}\right) \tag{2}$$

where C_0 and C_t are the chromium concentration (mg/L) at the inlet and outlet of the column, respectively, K_{AB} is the Adams-Bohart constant (L/mg·min), N_0 is the saturation concentration (mg/L), Z is the packed bed height (cm), v is the linear flow rate (cm/min), and t is time (min).

III) Yoon – Nelson model

$$Ln\left(\frac{C_t}{C_0-C_t}\right)=K_{YN}t-K_{YN}\tau \tag{3}$$

where C_0 and C_t are the chromium concentration (mg/L) at the inlet and outlet of the column, respectively, K_{YN} is the Yoon-Nelson constant (L/min), τ is time (min) required to decrease at 50% initial chromium concentration and t is time (min).

IV) Dose – Response model

$$Ln\left(\frac{C_t}{C_0-C_t}\right)=aLn(C_0Qt)-aLn(q_0w) \tag{4}$$

where C_0 and C_t are the chromium concentration (mg/L) at the inlet and outlet of the column, respectively, a is a parameter of the Dose-Response model, q_0 is the adsorption capacity (mg/g), w is the mass of adsorbent (g), Q is the volumetric flow (mL/min) and t is time (min).

By far the Bed Depth Service Time (BDST) model is the most used for scaling column adsorption process, it is based on breakthrough time and packed bed height and has the advantage of being described by linear Eq. (5).

$$t_b=\left(\frac{N_0}{C_0v}\right)Z-Ln\left(\frac{C_0}{C_b}\right)\left(\frac{1}{C_0K_a}\right) \tag{5}$$

where t_b is the service time at the breakthrough point (min), N_0 is the adsorption capacity (mg/L), C_0 is the initial chromium concentration (mg/L), C_b is the chromium concentration at breakthrough point (mg/L), v is the linear flow velocity (cm/min), Z is the packed bed height (cm), and K_a is the adsorption rate constant (L/mg·min). These parameters are calculated as a function of flow rate and chromium concentration, and then used to scale the adsorption process.

Due to the above, it is evident the need to propose a procedure to develop the technology for the removal of heavy metals through the continuous adsorption process in packed columns with abundant and low cost adsorbents. With this in mind, the aim of this work was to model and scale up the adsorption process of Cr(VI) ions using Mexicalcite as adsorbent in a packed column operating continuously. For this purpose, the work was divided into the following activities: i) the removal rates and adsorption capacity of Cr(VI) ions were determined as a function of packed bed height, flow rate and initial chromium concentration; ii) four different models were used to adjust the dynamic behavior of the column; and iii) the BDST model was used to scale the adsorption process in packed columns. It is expected that, in this way, the knowledge generated will contribute to the design of packed columns in continuous processes at industrial scale. These columns should be able to operate continuously at different flow conditions, packed bed heights and initial solute concentrations to efficiently remove heavy metals from industrial wastewater using natural adsorbent materials.

2. Materials and methods

2.1. Physicochemical properties of the adsorbent

Mexicalcite is a natural mineral obtained from mines located in Oaxaca, México; and marketed by Lumogral S.A. de C·V., Company (Mexico City). Its physicochemical characteristics reported by the company include 1604 kg/m^3 bulk density; particle sizes of 0.149–0.177 mm; 23.2% porosity; 4.5 μm pore diameter; 1132 m^2/kg surface area; 2.7 × 10^{-3} m/s permeability, and a pH value of 9.3 at zero-point charge.

2.2. Characterization of the adsorbent

The Mexicalcite mineral was washed with hot water at 40 °C and dried at 100 °C in an oven for 24 h. Then, SEM images and EDS spectra were obtained for elemental analysis using a JEOL model JSM6510LV electron microscope coupled to an EDS BRUKER QUANTAX model 200, with a resolution of 129 eV. Infrares analysis was carried out in a Bruker Tensor 27 model spectrometer in a range between 4000 and 400 cm^{-1} at 32 scans with ATR technique.

2.3. Preparation of Cr(VI) solutions

One liter of potassium dichromate ($K_2Cr_2O_7$) stock solution with a concentration of 100 mg/L was prepared. In one liter of distilled water, 283 mg of potassium dichromate (J.T. Baker, 99.9%), were dissolved. The pH of the solution was 7.1. Subsequently, by dilution in distilled water, the solutions with 75, 50 and 25 mg/L were prepared.

2.4. Determination of Cr(VI) in the effluent

Chromium concentration was determined by a standardized method using atomic absorption spectroscopy (AAS); in a VARIAN model 240FS spectrophotometer equipped with an acetylene burner and a hollow cathode lamp. The analysis was performed with a wavelength of 540 nm and a bandwidth 0.2 mm. Samples were analyzed in duplicate. The resulting chromium concentrations had relative errors of less than 5%.

2.5. Column Cr(VI) adsorption process

A glass column (1 cm diameter, 15 cm length) was used for the adsorption experiments. In addition, the upflow was performed and controlled by a peristaltic pump (Cole Parmer MasterFlex). The schematic representation of the adsorption process in the packed bed column used in this work is shown in Fig. 1.

The chromium concentration in the effluent (C_t) was measured every 15 min. Then, the concentration of adsorbed chromium was obtained from the value of the area under the curve of C_{ads} vs. time using Origin 8.0 data analysis software and incorporated into Eq. (6) to obtain the maximum column capacity of the column, q_{sat} (mg) [18].

$$q_{sat} = \frac{QA}{1000} = \frac{Q}{1000}\int_0^{t=t_{sat}} C_{ads}\,dt \tag{6}$$

where $C_{ads} = C_0 - C_t$, C_t is the chromium concentration at any time; t_{sat} is the saturation time in the column. A saturation concentration of $0.995C_0$ was considered; Q is the volumetric flow rate (mL/min) and A is the area under the curve (min•mg/L). The adsorption capacity, q (mg/g), is the maximum column capacity, q_{sat}, divided by the mass of the adsorbent, w (g) (Eq. (7)).

$$q = \frac{q_{sat}}{w} \tag{7}$$

The chromium mass (g) retained in the column at the saturation time, m_{sat} is as follows (Eq. (8)).

$$m_{sat} = \frac{C_0 Q t_{sat}}{1000} \tag{8}$$

The percentage of removal (%R) is obtained by means of Eq. (9):

$$\%R = \frac{q}{m_{sat}} \times 100 \tag{9}$$

The mass transfer zone, MTZ (cm) was also determined using Eq. (10).

$$MTZ = Z\left(1 - \frac{t_b}{t_{sat}}\right) \tag{10}$$

where t_b is the breakthrough time (min), namely the time required to reach 0.1 mg/L chromium concentration in the effluent. This value represents the tolerance limit for chromium discharges into surface waters [22].

The analysis of the parameters [the packed bed height (Z), volumetric flow (Q) and the initial concentration (C_0)], was performed according to the experiments shown in Table 1, where Z and Q parameters had three levels (2, 4 and 6, respectively), and C_0 parameter too (25, 50 and 75).

2.6. Effect of bed height on the continuous adsorption process

The effect of bed height was analyzed at three heights (Z = 2, 4 and 6

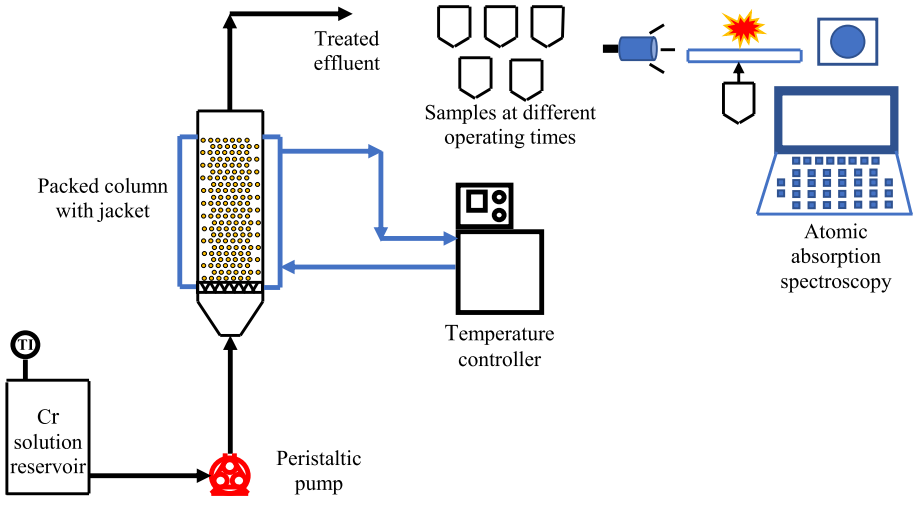

Fig. 1. Schematic representation of the packed bed column used in the Cr(VI) adsorption process.

Table 1
Experiments for the column chromium adsorption process.

Experiment number	Z (cm)	Q (mL/min)	C_0 (mg/L)
1	2	2	25
2	4	2	25
3	6	2	25
4	4	4	25
5	4	6	25
6	4	2	50
7	4	2	75

cm), maintaining C_0, Q and T at 25 mg/L, 2 mL/min and 20 °C, respectively.

2.7. Effect of flow rate and initial concentration on the continuous adsorption process

The effect of flow rate was analyzed at three levels, 2, 4, and 6 mL/min, maintaining at 4 cm the packed bed height, at 25 mg/mL the initial concentration and at 20 °C. While the effect of the initial concentration was analyzed at 25, 50 and 75 mg/L; maintaining the packed bed height of 4 cm, 2 mL/min volumetric flow rate and at 20 °C. For both parameters the analysis was performed as a function of breakthrough time. Finally, the experimental breakup time was compared with that obtained by the BDST model.

3. Results and discussion

3.1. Characterization of the adsorbent mineral before and after contact with the Cr(VI) solution

The surface morphology of the Mexicalcite mineral before and after contact with the chromium solution is shown in Fig. 2. It was not physically modified by the presence of chromium.

On the other hand, elemental analysis of the adsorbent composition before and after contact with chromium ions was carried out. Table 2 shows the mean values of each element recorded at four different points on the adsorbent surface. It can be observed that the Mexicalcite retained the chromium on its surface, which is probably due to the chemical interactions between the chromium ionic species and the oxygen of the silicon oxide, calcium oxide or calcium magnesium silicate groups present in this adsorbent. The presence of potassium can also be seen, which is related to the potassium dichromate used as a precursor salt of the chromium ions. Elemental analysis of each chemical component before and after contact with the chromium solution shows a slight increase in the concentration carbon and calcium, probably due to their presence in the water with the chromium solution was prepared.

Table 2
Elemental analysis for Mexicalcite before and after to the contact with chromium solution.

Element	Before		After	
	Mass (%)	Atom (%)	Mass (%)	Atom (%)
Oxygen	54.64	62.35	51.37	58.30
Carbon	12.41	18.78	16.44	24.54
Calcium	10.31	5.44	13.39	6.10
Silicon	10.15	6.61	7.95	5.16
Aluminium	4.64	3.14	3.20	2.16
Magnesium	3.24	2.47	1.78	1.01
Iron	2.51	0.82	1.84	0.60
Sodium	0.52	0.40	0.44	0.66
Potassium	0	0	1.84	0.85
Chromium	0	0	1.75	0.61

Elements such as sodium, aluminum, magnesium, silicon and iron are natural components of the Mexicalcite mineral; their amounts decrease after contact with the aqueous solution, probably due to the incorporation of chromium ions that replace some of the elements present on the surface of the Mexicalcite.

3.2. FTIR analysis

The functional groups responsible for the adsorption of Cr(VI) species on the surface of Mexicalcite, were identified by the analytical

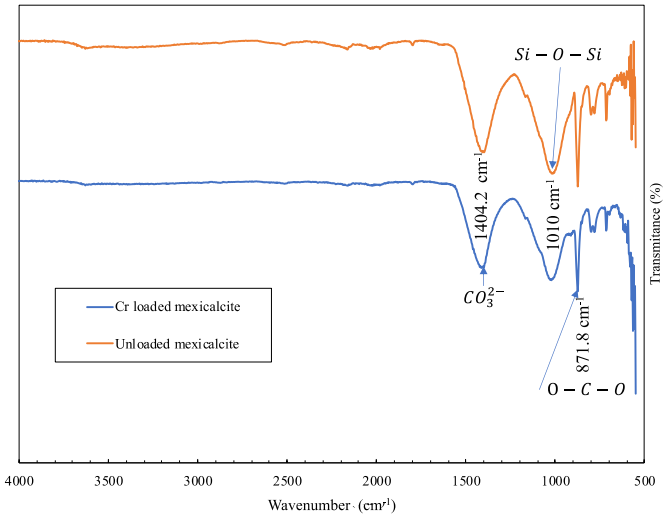

Fig. 3. FTIR spectra of unloaded and Cr(VI) loaded Mexicalcite.

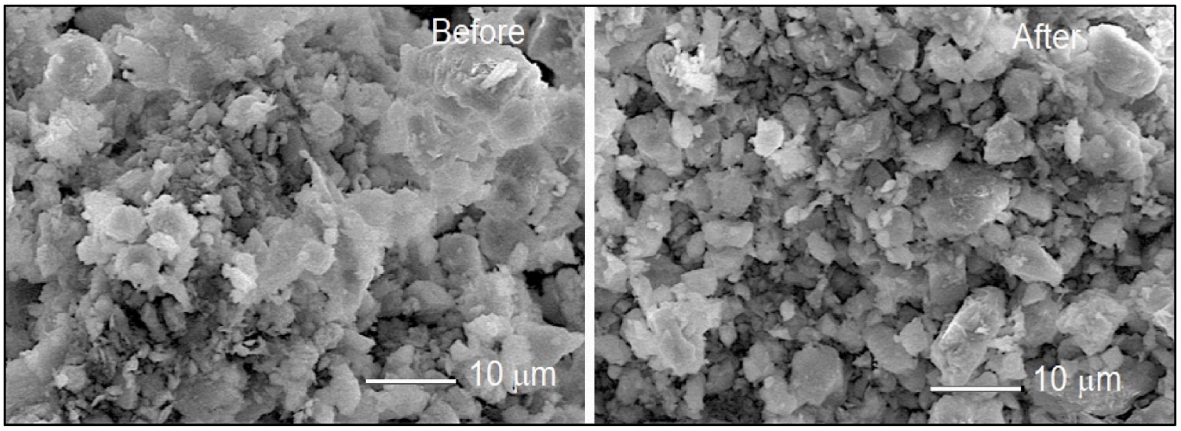

Fig. 2. SEM images for Mexicalcite mineral before and after to the contact with chromium solution.

technique of Fourier transform infrared spectroscopy (FTIR). Fig. 3 shows the spectra of Mexicalcite with and without Cr(VI) ions.

The corresponding values for each vibration band are shown in Table 3. According to the previously reported X-ray diffraction analysis, the main compounds present in Mexicalcite are Calcite, Quartz and Calcium and Magnesium Silicate [23]. The bands that indicate the presence of quartz are (1165, 1016, 798.5, 779.2, 694.4, 671.2, 586 and 555.5 cm^{-1}), calcite (1404.2, 871.8, 713.6 cm^{-1}) and Calcium and Magnesium Silicate (729.1, 725.2, and 578.6 cm^{-1}), [24–26].

The peaks at wavelengths 718, 875 and 1425 cm^{-1} correspond to asymmetric bending and stretching vibrations of calcite [8,27], which do not show any shift changes. However, where the presence of chromium is clearly appreciated is in the band shift from 798 to 794 cm^{-1} corresponding to the O–Si – O bending vibrations and in another band shift from 1010 to 1018 cm^{-1} in the symmetric stretching vibration of the Si–O – Si functional group [16,28].

These results allow concluding that the Chromium interactions occur mainly on the oxygen present in the silicate portion of the Mexicalcite, and that there is no interaction with the calcite groups, this behavior has been previously seen by other researchers in similar compounds, where they relate the shifts in the symmetrical stretching vibration with the interactions between chromium and the Si–O group [10,28]. It can also be concluded that there is no appreciable interaction with the oxygen present in the carbonate groups of calcite, since none of these peaks undergo any displacement, they remain the same between the unloaded and chromium-loaded samples.

3.3. Modeling of the continuous process

The results of the breakthrough time (t_b) as a function of packed bed height (Z), had a satisfactory fit ($R^2 = 0.9998$); which allowed to achieve the linear equation.

$$t_b = 106.08Z - 64.39 \tag{11}$$

For a flow rate of 2 mL/min and an initial chromium concentration of 25 mg/L adsorption capacity (N_0) and the adsorption rate constant (K_a) were obtained for the BDST model, with values of 6753.25 mg/L and 0.0034 L/mg•min, respectively. Considering a cylindrical column, it is possible to achieve the breakthrough time equation for each set of Z, Q and C_0 values, as follow. Considering a cylindrical column with area = $(\pi/4)\ d^2$, where d is the internal diameter, and the BDST model, it was possible to achieve the following expression.

$$t_b = \left(\frac{6753.25\ \pi\ d^2}{4C_0Q}\right)Z - Ln\left(\frac{C_0}{0.1}\right)\left(\frac{1}{0.0034C_0}\right) \tag{12}$$

Table 3
FTIR analysis of unloaded and Cr(VI) loaded Mexicalcite.

Functional groups	Mexicalcite, cm^{-1}	Cr(VI) loaded Mexicalcite, cm^{-1}
Surface –OH stretching vibrations	3626	3626
CO_3^{2-} asymmetrical stretching	1404.2	1404.2
Si–O asymmetrical stretching	1165	1165
Si–O – Si symmetrical stretchig	1010	1018
O–C – O bending in-plane deformation	871.8	871.8
O–Si – O bending vibrations	798	794
Si–O symmetrical stretching	779.2	779.2
Ca–CO_3 – Mg	725.2	729.1
O–C – O asymmetric bending	713.6	713.6
Si–O symmetrical bending	694.4	694.4
Si–O – Si bending vibrations	671.2	671.2
Si–O stretching, Si–O–Al stretching	586.4	582.5
Ca = O	578.6	578.6
Si–O bending, Si–O–Al stretching	555.5	555.5

The above equation was used to obtain calculated breakthrough time ($t_{b\ cal}$), for each experimental set of Z, Q and C_0 values, by means of Microsoft Excel Solver tool or Polymath 6.1 software. Then, both $t_{b\ cal}$ and $t_{b\ exp}$, are compared, whose values are shown in Table 4. The relative deviation (ARD) was added; its values were less than 2%, confirming the effectiveness of the model.

The results of the continuous chromium adsorption process are shown in Table 5, the highest removal percentage were obtained, varying from 72.17 to 94.09%, as well as adsorption capacities, from 4.9 to 5.13 mg/g. These values are higher than those reported for natural zeolites such as Erionite (0.103 mg/g), Cowlesite (0.763 mg/g), Willhendersonite (0.719 mg/g) and modified Clinoptilolite (3.83 mg/g) [13].

The best column operating conditions were those obtained in experiment 3, in which the chromium concentration decreased from 25 to 0.1 mg/L, in a packed bed column containing 5.986 g of adsorbent; processing 1305 mL of effluent in a mass transfer zone of 0.24 cm. As can be seen in Table 6, the column saturation time was 652.5 min and the time to reach 50% ($t_{50\%}$) less than the initial concentration was 613.7 min. On average, this parameter has a relative deviation of less than 1% between the value obtained experimentally and that calculated by the Yoon-Nelson model.

3.4. Modeling of breakthrough curves

The most widely used models to model the dynamic behavior of column adsorption processes, include I) Thomas; II) Adams-Bohart; III) Yoon-Nelson and IV) Dose-Response. Table 7 shows the results for each parameter according to the select model. They show a good coefficient of determination with $R^2 > 0.99$. The linear fit of the experimental data with the models represented by the 1, 2, 3 and 4 equations was satisfactory. According to the average absolute relative deviation (AARD) parameter, values below 8% were obtained using the Thomas, Adams-Bohart and Yoon Nelson models; not so for Dose-Response model, whose value was higher than 20%. Thus, removal of chromium by the mineral Mexicalcite in a packed bed column is carried out through an adsorption – desorption process without axial dispersion and slowly reaching equilibrium [20,29].

3.5. Effect of the packed bed height

By doubling and tripling the packed bed height; the amount of adsorbent material inside the column (w), the time to reduce the initial concentration to 50% ($t_{50\%}$) and the saturation time, doubled and tripled in the same proportion, as can be seen in Table 5 (experiments 1, 2 and 3). This effect can be seen graphically in Fig. 4. According to the breakthrough curve, it is easy to identify the typical “S" shape in the curve (Fig. 4). This “S" shape curve is achieved in processes where small particle size distributions are used [21]. The results were favorable, as the removal rate increased by 7.5%, the adsorption capacity by 2.3% and the effluent volume by 66%, but the mass transfer zone decreased by 43%. In summary, increasing the amount of adsorbent material results in an increase in surface area and the number of available active sites facilitating the adsorption process. In addition, the increase in contact time favors the mass transfer phenomenon [30]. This behavior has been

Table 4
Comparison of $t_{b\ exp}$ and $t_{b\ cal}$ by using the BDST model.

Experiment number	$t_{b\ exp}$ (min)	$t_{b\ cal}$ (min)	ARD (%)
1	149.60	147.77	1.22
2	356.23	359.93	1.04
3	573.90	573.09	0.14
4	147.47	147.77	0.20
5	78.40	77.05	1.72
6	177.06	175.91	0.65
7	115.90	115.69	0.18

Table 5
Removal percentage and adsorption capacity for Mexicalcite.

Experiment number	R %	q (mg/g)
1	81.57	4.90
2	90.72	4.99
3	94.09	5.13
4	80.66	4.92
5	72.17	4.92
6	91.30	5.01
7	89.76	4.96

Table 6
Experimental parameters of Cr(VI) adsorption with Mexicalcite in a packed bed column.

Experiment number	w (g)	$t_{50\%}$ (min)	t_s (min)	V_{eff} (mL)	MTZ (cm)
1	1.995	195.5	239.68	479.36	0.75
2	3.991	398.3	439.39	878.78	0.38
3	5.986	613.7	652.52	1305.04	0.24
4	3.991	196.7	243.56	974.24	1.58
5	3.991	130.7	181.36	1088.16	3.41
6	3.991	201.5	218.9	437.8	0.38
7	3.991	135.0	147.04	278.2	0.42

reported by other authors, who explain that the increase in breakthrough time with packed bed height is due to longer contact time, since amount of adsorbent increases surface area and therefore the number of available sites for adsorption [20,30].

3.6. Effect of flow rate

Fig. 5 shows the breakthrough curves for the flow rates. The flow rate affects the percentage removal more than the adsorption capacity, the latter remains almost constant. As the flow rate increased from 2 to 4, and from 4 to 6 mL/min, the percentage removal decreased by 11% on average. Since the mass transfer rate is slower than the flow rate, a larger surface area is required to achieve chromium removal, this phenomenon is reflected in an increase of the mass transfer zone (MTZ). This increases from 0.38 cm to 3.41 cm when the flow rate increases from 2 to 6 mL/min. In summary, the contact time decreases with increasing flow increases. Therefore, the breakthrough time is very short and column

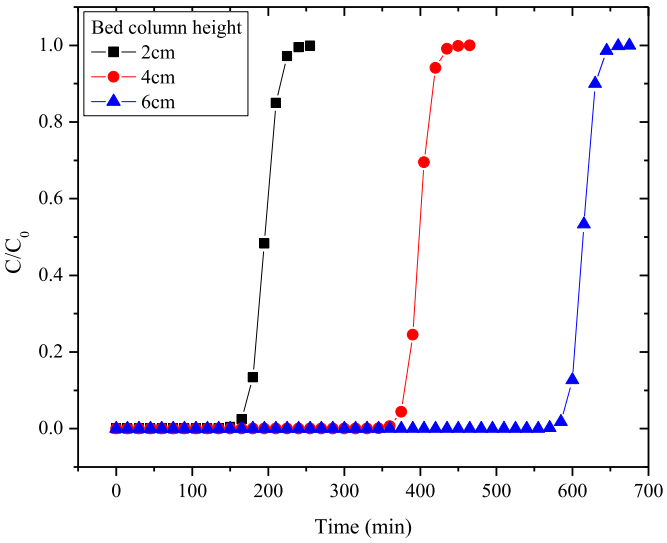

Fig. 4. Breakthrough curves as a function of the bed heights (Q = 2 mL/min, C_0 = 25 mg/L).

Table 7
Column adsorption process parameters according to the used models.

Model	Experiment number	q_0 (mg/g)	K_{Th} (mL/mg·min)	R^2	AARD (%) for C_{exp} vs C_{cal}
Thomas	1	4.768	4.897	0.999	3.05
	2	5.156	4.991	0.998	5.71
	3	5.528	5.129	0.999	2.47
	4	4.544	4.928	0.997	6.30
	5	4.224	4.923	0.998	2.13
	6	5.418	4.998	0.997	9.33
	7	5.103	5.007	0.999	1.60
Model	**Experiment number**	**N_0 (mg/L)**	**K_{A-B} (mL/mg min)**	**R^2**	**AARD (%) for C_{exp} vs C_{cal}**
Adams – Bohart	1	6273.718	4.668	0.998	3.70
	2	6377.797	4.998	0.994	8.73
	3	6516.739	5.528	0.996	6.31
	4	6243.628	4.592	0.995	11.6
	5	6295.498	4.188	0.995	9.64
	6	6398.443	5.19	0.993	10.06
	7	6357.898	5.123	0.998	2.08
Model	**Experiment number**	**τ (min)**	**K_{Y-N} (min^{-1})**	**R^2**	**AARD (%) for C_{exp} vs C_{cal}**
Yoon – Nelson	1	195.529	0.119	0.999	2.51
	2	398.417	0.1289	0.998	5.71
	3	614.088	0.1382	0.999	2.47
	4	196.673	0.1136	0.997	5.82
	5	130.994	0.1056	0.998	3.48
	6	199.476	0.2709	0.997	6.33
	7	133.214	0.3827	0.999	1.60
Model	**Experiment number**	**q_0 (mg/g)**	**a**	**R^2**	**AARD (%) for C_{exp} vs C_{cal}**
Dose – Response	1	4.800	22.661	0.992	18.11
	2	4.953	48.539	0.994	22.90
	3	5.115	82.521	0.991	10.01
	4	4.773	20.871	0.989	23.79
	5	4.697	13.211	0.982	21.03
	6	4.942	51.803	0.993	22.24
	7	4.944	50.703	0.996	22.40

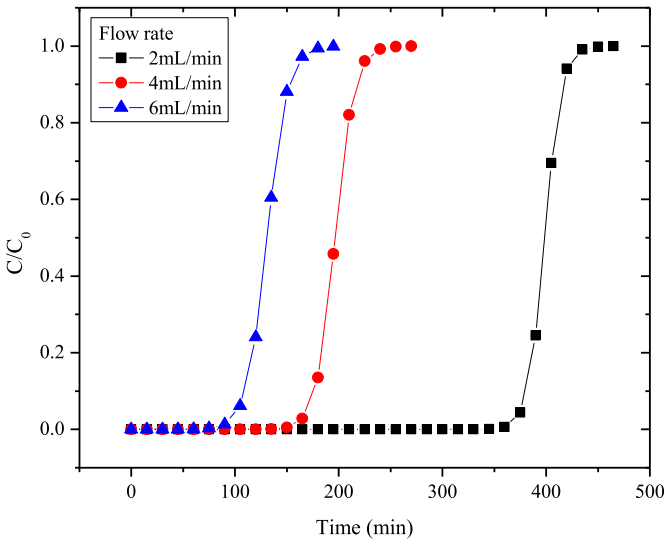

Fig. 5. Breakthrough curves as a function of flow rates (Z = 4 cm, C_0 = 25 mg/L).

saturation is reached quickly [31].

3.7. Effect of initial concentration

The shapes of the breakthrough curves at different inlet concentration are shown in Fig. 6. The variation of the initial concentration has little effect on the removal rate and adsorption capacity, which remain practically constant when the chromium concentration is doubled and tripled. The greatest effect is on the effluent volume, since increasing the chromium concentration at the column inlet from 25 to 50 and from 50 to 75 mg/L reduces the effluent volume by 43% on average. The breakthrough time and saturation time decrease with increasing concentration. Thus, adsorption is very fast, due to the large driving force produced by the chromium concentration gradient between the liquid phase and the adsorbent surface. Unfortunately, a large amount of chromium ions in the system quickly depletes the active sites of the adsorbent, causing saturation on the column in a short time [32].

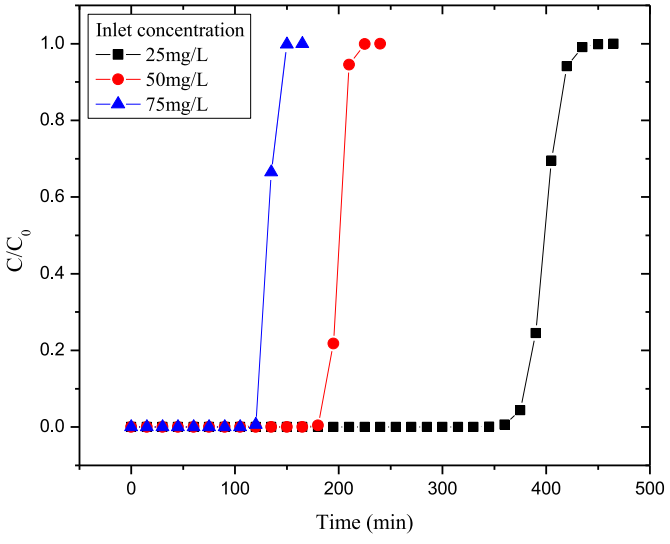

Fig. 6. Breakthrough curves as a function of the initial concentrations (Q = 4 mL/min, Z = 4 cm).

3.8. Comparison of $t_{b\ exp}$ and $t_{b\ cal}$ in a real scaling process

To validate the BDST model represented by Eq. (12), three experiments were performed on a 2 cm diameter column (original column diameter was 1 cm), with a bed height/column diameter ratio (Z/d) equal to 2. The amount of adsorbent for a packed bed height of 4 cm was 15.964 g with a void fraction of 20.8%. In these experiments, the time required to reach a chromium concentration of 0.1 mg/L at the column outlet was determined using different combinations of flow rate and initial concentration. Table 8 shows the experimental and calculated values for the breakthrough time. Comparing the breakthrough time values of experiments 8, 9 and 10, it can be observed that the average relative deviation (ARD) is less than 1%, which validates the use of Eq. (12) as a suitable model to scale the adsorption process.

3.9. Examples of scaling process

Once the model represented by Eq. (12) was validated; it was used to obtain the column dimensions for the ratio $Z/d = 2$. The objective was to obtain the packed bed height (Z) and the column diameter (d), to reduce initial chromium concentration to 0.1 mg/L in 120 h of continuous operation time. The results are shown in Table 9. For example, a column of 40.83 cm diameter with 81.66 cm packed bed height, containing 135.8 kg of Mexicalcite as adsorbent, is theoretically capable of removing 99.9% of the chromium from solution with an initial concentration of 100 mg/L, with a feed flow of 1 L/min for 120 h (5 days), reaching an effluent volume of 7200 L. These results were obtained with Eq. (12), using Excel Solver program or Polymath 6.1 software. For 7200 min of breakthrough time, the value of Z_{cal} was obtained, giving arbitrary values to the column diameter but keeping the relation Z/d = 2.

The adsorption capacity values obtained for examples 1, 2 and 3 in Table 9 were 5.25, 5.28 and 5.30 mg/g, respectively. These results show an average relative deviation of 4.3% with respect to the average value obtained experimentally (4.98 mg/g). Therefore, the validation of the scaling model is once again confirmed.

3.10. Comparison of Cr(VI) removal results in columns packed with other adsorbents

Table 10 shows the values of adsorption capacity and percentage removal of Cr(VI) obtained in columns packed with different adsorbents. In all cases, the maximum adsorption percentage is reported, which was achieved with the best column operating conditions. According to most authors, this is achieved by operating the column with the lowest volumetric flow rate, the lowest initial chromium concentration, and the highest packed bed height [22,27,33]. Then, the differences in the values of adsorption capacity and percentage removal shown by the different adsorbents are due to the type of Cr(VI) species adsorbed, the pH of the aqueous chromium solution and the nature of the adsorbent, which is related to the pH of its point of zero charge (pH_{pzc}) rather than to the surface area value. In this regard, it has been reported that the effect of porosity and surface area on the adsorption capacity and % removal is small when the adsorbent material has low porosity and small surface area, in these cases the role of pore filling in the chromium adsorption process is negligible [39].

Table 8
Experimental and calculated breakthrough time in a real scaling process.

Experiment number	Z/d ratio	Q (mL/min)	C_0 (mg/L)	$t_{b\ exp}$ (min)	$t_{b\ cal}$ (min)	ARD (%)
8	2	2	25	776.64	784.25	0.98
9	2	6	25	505.58	501.37	0.83
10	2	2	75	537.21	540.02	0.52

Table 9
Column dimensions calculated by the BDST model for 120 h continuous operation.

Scaling example	Q (mL/min)	C_0 (mg/L)	w (g)	Z_{cal} (cm)	d_{column} (cm)	Z/d	V_{eff} (L)	$w_{Cr\ ads}$ (mg)
1	10	25	341.6	11.12	5.55	2.00	72	1793
2	100	50	6806.1	30.22	15.05	2.00	720	35,928
3	1000	100	135,819.8	81.66	40.83	2.00	7200	719,280

Table 10
Comparison of adsorption capacity and maximum % removal of Cr(VI) with different adsorbents in packed bed columns.

Adsorbent	Surface area (m^2/g)	pzc pH	Cr solution pH	q (mg/g)	Removal (%)	Reference
Mexicalcite	1.13	9.3	7	5.13	94.1	This work
Rice bran	0.12	6.1	2	19.81		[33]
Activated charcoal (*Sapindus trifoliate* L)	201.11	7.2	7	1.719		[16]
Sago bark			3	35.82	89.55	[34]
Almond shell			3.7	21.92	65.88	[35]
Dolochar			2		88.5	[36]
Rice husk	0.54	6.05	2	11.04[a]		[27]
Psidium guajava leaves	7.7	6.05		18.32[a]		[8]
Rice husk ash		6	2.5	44.4	89.3	[30]
ZeoliteNaX			4	5.66	84.99	[37]
Modified *Swietenia mahagoni* shell			2	10.827	69.04	[22]
Coconut shell	0.52	6.62	2	16.009		[17]
Neem leaf	0.57	6.94	2	14.08		[17]
Activated neem bark			2	28.89	72.89	[38]

[a] From Thomas model.

As can be seen from the results in Table 10, there is no direct relationship between surface area and adsorption capacity, unlike what happens with the pH of the solution, where it is observed that the higher the pH, the lower the adsorption capacity.

According to the relative distribution diagram of Cr(VI) species in water as a function of pH and Cr(VI) concentration reported in the literature [39], if the concentration is less than 1000 mg/L, the species mainly found in aqueous solution of pH < 1, 1 < pH < 6.5 and pH > 6.5 are H_2CrO_4, $HCrO_4^-$ and CrO_4^{2-}, respectively. The H_2CrO_4 and $HCrO_4^-$ species consume only one adsorption site, while the CrO_4^{2-} species requires two adsorption sites, but this species can be adsorbed by electrostatic interaction [33].

In the distribution diagram of Cr(VI) species at 75 mg/L (Fig. 7), it is observed that the species that predominates at pH = 7 is CrO_4^{2-} with 96%, which favors adsorption on Mexicalcite.

In the chromium adsorption process with Mexicalcite, a chromium solution with a maximum concentration of 75 mg/L and pH = 7 was used. Under these conditions, the surface of this adsorbent is still covered with H_3O^+ ions, and it can continue to adsorb chromate ions (CrO_4^{2-}) until it reaches its maximum capacity. Therefore, due to its high pH value at the point of zero charge (pHpzc = 9.3) presented by Mexicalcite, it is possible to operate the column with solutions with higher pH than using bioadsorbents (pHpzc <7), this represents an advantage because the effluent does not require neutralization treatment.

4. Conclusions

The natural mineral known as Mexiclacite turned out to be a material that has sorption capacity to remove Cr(VI) ions from aqueous solutions due to the chemical interaction that occurs between the Cr(VI) ions with the Si–O groups of the silica portion containing this mineral. As mexicalcite is insoluble in water, has a low swelling index and good mechanical strength properties, it was possible to use it efficiently in packed columns operating continuously under different operating conditions such as effluent flow, packed bed height and concentrations, both at laboratory and pilot scale. At laboratory scale, an average adsorption capacity of 4.98 mg/g was obtained for this adsorbent, and a chromium removal rate of 94.09% in an aqueous solution with an initial concentration of 25 mg/L, operating at a flow rate of 2 mL/min and a packed bed height of 6 cm in a column of 1 cm internal diameter. The effect of packed bed height, flow rate and initial concentration is evident in the column breakthrough and saturation time. This is not reflected in the adsorption capacity, but in the removal percentage, since increasing the packed bed height increases the breakthrough and saturation time, increasing the removal percentage. The opposite results were obtained when the flow rate was increased, since the reduction in contact time produces a greater reduction in the removal percentage. In this case, the variation of the initial concentration had no significant effect on the removal percentage. The three models: Thomas, Adams-Bohart and Yoon-Nelson, satisfactorily describe the continuous process in this system, according to the results of the %AARD, which compares the concentrations, experimental and calculated. The BDST model is suitable for scaling up the chromium adsorption process in a packed bed column. By doubling the column diameter, the percentage deviation was less than 1%, between the breakthrough time calculated with the BDST model and the experimental one.

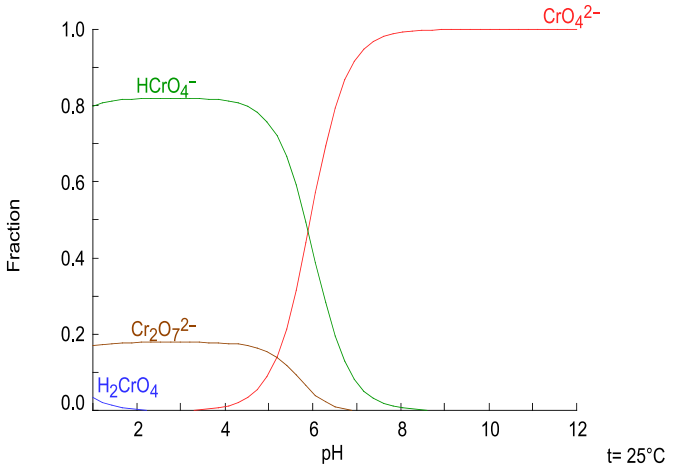

Fig. 7. Distribution diagram of Cr(VI) species at 75 mg/L and 0.637 M ionic strength.

Credit author statement

Julian Cruz-Olivares: Project administration and Writing- Original draft preparation César Pérez-Alonso: Supervision, Gonzalo Martínez-Barrera: Writing- Reviewing and Editing, abriela Roa-Morales: Methodology and Experiments, Gustavo López-Téllez: Characterization analysis techniques, Eduardo Martín del Campo-López. Methodology, Software.

Declaration of competing interest

The authors declare that they have no known competing financial interests or personal relationships that could have appeared to influence the work reported in this paper

References

[1] J.P. Wise Jr., J.L. Young, J. Cai, L. Cai, Current understanding of hexavalent chromium Cr(VI) neurotoxicity and new perspectives, Environ. Int. 158 (2022) 1–18, https://doi.org/10.1016/j.envint.2021.106877.

[2] S.P. den Braver-Sewradj, J.V. Benthem, Y.C.M. Staal, J. Ezendam, A.H. Piersma, E. V.S. Hessel, Occupational exposure to hexavalent chromium. Part II. Hazard assessment of carcinogenic effects, Regul. Toxicol. Pharmacol. 126 (2021) 1–19, https://doi.org/10.1016/j.yrtph.2021.105045.

[3] M. Khadem, F. Golbabaei, A. Rahmani, Occupational exposure assessment of chromium (VI): a review of environmental and biological monitoring, Int. J. Occup. Hyg. 9 (2017) 118–131. https://ijoh.tums.ac.ir/index.php/ijoh/article/view/290.

[4] R. Welling, J.J. Beaumont, S.J. Petersen, G.V. Alexeeff, C. Steinmaus, Chromium VI and stomach cancer: a meta-analysis of the current epidemiological evidence, J. Occup. Environ. Med. 72 (2015) 151–159, https://doi.org/10.1136/oemed-2014-102178.

[5] E.T. Wahyuni, N.P. Diantariani, I. Kartini, A. Kuncaka, Enhancement of the photostability and visible photoactivity of ZnO photocatalyst used for reduction of Cr(VI) ions, Res. Eng. 13 (2022) 1–8, https://doi.org/10.1016/j.rineng.2022.100351.

[6] A. Deepa, P. Prakash, B.K. Mishra, Performance of biochar-based filtration bed for the removal of Cr(VI) from pre-treated synthetic tannery wastewater, Environ. Technol. 42 (2021) 257–269, https://doi.org/10.1080/09593330.2019.1626912.

[7] J. Bayuo, An extensive review on chromium (VI) removal using natural and agricultural wastes materials as alternative biosorbents, J. Environ. Health Sci. Eng. (2021), https://doi.org/10.1007/s40201-021-00641-w.

[8] T. Mitra, S.K. Das, Cr(VI) removal from aqueous solution using Psidium guajava leaves as green adsorbent: column studies, Appl. Water Sci. 9 (2019) 153, https://doi.org/10.1007/s13201-019-1029-2.

[9] A. Das, N. Bar, S.K. Das, Adsorptive removal of Pb(II) ion on Arachis hypogaea's shell: batch Experiments, statistical, and GA modeling, Int. J. Environ. Sci. Technol. (2022), https://doi.org/10.1007/s13762-021-03842-w.

[10] B. Singha, N. Bar, S.K. Das, The Use of Artificial Neural Networks (ANN) for Modeling of Adsorption of Cr(VI) Ions, Desalin. Water Treat., 2013, pp. 1–11, https://doi.org/10.1080/19443994.2013.813682.

[11] A. Das, M. Banerjee, N. Bar, S.K. Das, Adsorptive removal of Cr(VI) from aqueous solution: kinetic, isotherm, thermodynamics, toxicity, scale-up design, and GA modeling, SN Appl. Sci. 1 (2019) 776, https://doi.org/10.1007/s42452-019-0813-9.

[12] S.P. Dubey, K. Gopal, Adsorption of chromium(VI) on low cost adsorbents derived from agricultural waste material: a comparative study, J. Hazard Mater. 145 (2007) 465–470, https://doi.org/10.1016/j.jhazmat.2006.11.041.

[13] C. Rosales-Landeros, C.E. Barrera-Díaz, B. Bilyeu, V. Varela-Guerrero, F. Ureña-Núñez, A review on Cr(VI) adsorption using inorganic materials, Am. J. Anal. Chem. 4 (2013) 8–16, https://doi.org/10.4236/ajac.2013.47A002.

[14] S. Bensaadi, N. Drai, O. Arous, Y. Berbar, Z.E. Hammache, M. Amara, B. Van der Bruggen, A study of chromium (VI) ions fixation and transport using polymer inclusion membrane containing D2EHPA as complexing agent, J. Membr. Sci. Res. 8 (2022) 1–7, https://doi.org/10.22079/JMSR.2021.531653.1470.

[15] J.J. Jacob, R. Varalakshmi, S. Gargi, M.A. Jayasri, K. Suthindhiran, Removal of Cr (III) and Ni (II) from tannery effluent using calcium carbonate coated bacterial magnetosomes, npj Clean Water 1 (2018), https://doi.org/10.1038/s41545-018-0001-2.

[16] S. Mohanta, M.K. Sahu, P.C. Mishra, A.K. Giri, Removal of Cr (VI) from aqueous solution by activated charcoal derived from Sapindus trifoliate L fruit biomass using continuous fixed bed column studies, Water Sci. Technol. 84 (2021) 55–65, https://doi.org/10.2166/wst.2021.217.

[17] S. Sarkar, S. Das, Removal of hexavalent chromium from aqueous solution using natural adsorbents-column studies, Int. J. Eng. Technol. Res. 5 (2016) 370–377, https://doi.org/10.17577/IJERTV5IS110270.

[18] J. Cruz-Olivares, C.E. Barrera-Díaz, G. Martínez-Barrera, C. Pérez-Alonso, G. Roa-Morales, Comparative application of an irradiated and non-irradiated calcite-type material to improve the removal of Pb in batch and continuous processes, J. Environ. Chem. Eng. 6 (2018) 6297–6307, https://doi.org/10.1016/j.jece.2018.09.051.

[19] E. Palma-Anaya, Ch Fall, T. Torres-Blancas, P. Balderas-Hernández, J. Cruz-Olivares, C.E. Barrera-Díaz, G. Roa-Morales, Pb(II) removal process in a packed column system with xanthation-modified deoiled allspice husk, J. Chem. (2017), https://doi.org/10.1155/2017/4296515.

[20] H. Patel, Fixed-bed column adsorption study: a comprehensive review, Appl. Water Sci. 9 (2019) 1–37, https://doi.org/10.1007/s13201-019-0927-7.

[21] J. Cruz-Olivares, C. Pérez-Alonso, C. Barrera-Díaz, Fernando Ureña-Nuñez, M. C. Chaparro-Mercado, Bilyeu Bryan, Modeling of lead (II) biosorption by residue of allspice in a fixed-bed column, Chem. Eng. J. 228 (2013) 21–27, https://doi.org/10.1016/j.cej.2013.04.101.

[22] S. Rangabhashiyam, M.S. Giri Nandagopal, E. Nakkeeran, N. Selvaraju, Adsorption of hexavalent chromium from synthetic and electroplating effluent on chemically modified Swietenia mahagoni shell in a packed bed column, Environ. Monit. Assess. 18 (2016) 1–13, https://doi.org/10.1007/s10661-016-5415-z.

[23] J. Cruz-Olivares, G. Martínez-Barrera, C. Pérez-Alonso, C.E. Barrera-Díaz, M. C. Chaparro-Mercado, F. Ureña-Núñez, Adsorption of lead ions from aqueous solutions, J. Chem. (2016) 1–7, https://doi.org/10.1155/2016/8782469.

[24] S. Hajji, T. Turki, A. Boubakri, M.B. Amor, N. Mzoughi, Study of Cadmium Adsorption onto Calcite Using Full Factorial Experiment Design, Desalin. Water Treat., 2017, pp. 1–12, https://doi.org/10.5004/dwt.2017.21079.

[25] G. Jozanikohan, M.N. Abarghooei, The Fourier transform infrared spectroscopy (FTIR) analysis for the clay mineralogy studies in a clastic reservoir, J. Pet. Explor. Prod. Technol. 12 (2022) 2093–2106, https://doi.org/10.1007/s13202-021-01449-y.

[26] F. Bosch Reig, J.V. Gimeno Adelantado, M.C.M. Moya Moreno, FTIR quantitative analysis of calcium carbonate (calcite) and silica (quartz) mixtures using the constant ratio method. Application to geological samples, Talanta 58 (2002) 811–821, https://doi.org/10.1016/S0039-9140(02)00372-7.

[27] T. Mitra, N. Bar, S.K. Das, Rice husk: green adsorbent for Pb(II) and Cr(VI) removal from aqueous solution-column study and GA–NN modeling, SN Appl. Sci. 1 (2019) 486, https://doi.org/10.1007/s42452-019-0513-5.

[28] T.K. Naiya, B. Singha, S.K. Das, FTIR study for the Cr(VI) removal from aqueous solution using rice waste, international conference on chemistry and chemical process, Int. Proc. Chem. Biol. Environ. Eng. 10 (2011) 114–119. https://www.researchgate.net/publication/308328135.

[29] A.D. Dorado, X. Gamisans, C. Valderrama, M. Sole, C. Lao, Cr(III) removal from aqueous solutions: a straightforward model approaching of the adsorption in a fixed-bed column, J. Environ. Sci. Health, Part A 49 (2014) 179–186, https://doi.org/10.1080/10934 529.2013.83885 5.

[30] S.M. Yakout, M.R. Hassanc, H.A. Omar, Fixed-bed column study for the removal of hexavalent chromium ions from aqueous solutions via pyrolysis of rice husk, Desalination Water Treat. 170 (2019) 128–137, https://doi.org/10.5004/dwt.2019.24468.

[31] L. Sheng, Y. Zhang, F. Tang, S. Liu, Mesoporous/Microporous Silica Materials: preparation from natural sands and highly efficient fixed-bed adsorption of methylene blue in waste water, Microporous Mesoporous Mater. 257 (2018) 9–18, https://doi.org/10.1016/j.micomeso.2017.08.023.

[32] A. Saravanan, P. Senthil Kumar, M. Yaswanthraj, Modelling and analysis of packed bed column for the effective removal of zinc from aqueous solution using dual surface modified biomass, Part. Sci. Technol. 36 (2017) 934–944, https://doi.org/10.1080/02726351.2017.1329243.

[33] S. Sarkar, N. Bar, S.K. Das, Cr(VI) and Cu(II) removal from aqueous solution in fixed bed column using rice bran; experimental, statistical and GA modelling, J. Indian Chem. Soc. 98 (2021) 1–9, https://doi.org/10.1016/j.jics.2021.100216.

[34] S. Fauzia, H. Aziz, D. Dahlan, R. Zein, Modelling for removal of Cr(VI) and Pb(II) using sago bark (Metroxylon sagu) by fixed-bed column method, Egypt, J. Chem. 64 (2021) 3981–3989, https://doi.org/10.21608/EJCHEM.2020.20172.2212.

[35] M.D. Yahya, H. Abubakar, K.S. Obayomi, Y.A. Iyaka, B. Suleiman, Simultaneous and continuous biosorption of Cr and Cu (II) ions from industrial tannery effluent using almond shell in a fixed bed column, Res. Eng. 6 (2020), 100113, https://doi.org/10.1016/j.rineng.2020.100113.

[36] N. Tiadi, R.R. Dash, C.R. Mohanty, A.M. Patel, Comparative studies of adsorption of chromium(VI) ions onto different industrial wastes, J. Hazard. Toxic Radioact. Waste 24 (2020), 04020021, https://doi.org/10.1061/(ASCE)HZ.2153-5515.0000517.

[37] P.K. Pandey, S.K. Sharma, Removal of Cr(VI) and Pb(II) from wastewater by ZeoliteNaX in fixed bed column, Water Conserv. Sci. Eng. 2 (2017) 61–65, https://doi.org/10.1007/s41101-017-0026-2.

[38] U. Maheshwari, S. Gupta, Removal of Cr(VI) from wastewater using activated neem bark in a fixed-bed column: interference of other ions and kinetic modelling studies, Desalination Water Treat. 57 (2016) 1–12, https://doi.org/10.1080/19443994.2015.1030709.

[39] H.N. Tran, D.T. Nguyen, G.T. Le, F. Tomul, E.C. Lima, S.H. Woo, A.K. Sarmah, H. Q. Nguyen, P.T. Nguyen, D.D. Nguyen, T.V. Nguyen, S. Vigneswaran, D.-V.N. Vo, H.-P. Chao, Adsorption mechanism of hexavalent chromium onto layered double hydroxides-based adsorbents: a systematic in-depth review, J. Hazard Mater. 373 (2019) 258–270, https://doi.org/10.1016/j.jhazmat.2019.03.018.